CHANDRA SPECTROIMAGERY OF THE GALAXY CLUSTER ABELL 1995

J.P. HUGHES
Department of Physics and Astronomy, Rutgers University, 136 Frelinghuysen Road, Piscataway, NJ, 08854 USA

S.K. PATEL, M. JOY
Department of Space Science, NASA Marshall Space Flight Center, Huntsville, AL, 35812 USA

J.E. CARLSTROM
Department of Astronomy and Astrophysics, University of Chicago, Chicago, IL, 60637 USA

Abell 1995 is a rich massive galaxy cluster at a redshift of 0.322 that we observed with the *Chandra X-ray Observatory* for ∼50 ks. We carried out a preliminary spectral and image analysis of the cluster in order to quantify its large and small scale density and temperature structure. Within the central arcminute or so, the three spectral bands show subtly different cluster morphologies. We also comment on the serendipitous point source content of the cluster field.

1 Introduction

We have been studying the X-ray emission and Sunyaev-Zel'dovich Effect (SZE) of a sample of rich galaxy clusters at modest redshifts ($z \sim 0.2 - 0.8$) in order to constrain cosmological parameters. In this article we report on a preliminary analysis of new *Chandra* X-ray data on the rich massive cluster Abell 1995 that lies at a redshift $z = 0.322$. This work is a follow-on to our earlier study of A1995 using *ROSAT* and *ASCA* data which appeared in Patel et al.[1] In the following we assume a cosmology with $\Omega_M = 0.3$, $\Omega_\Lambda = 0.7$, and $H_0 = 50\,h_{50}\,\mathrm{km\,s^{-1}\,Mpc^{-1}}$. Thus $1'$ equals $400\,h_{50}^{-1}$ kpc at the cluster.

2 Observations

Chandra observed A1995 for 45 ks in May 2000 and for an additional 12 ks in July 2000. The pointing direction was chosen so that the cluster was centered on the backside-illuminated chip (S3) of the Advanced CCD Imaging Spectrometer (ACIS-S).[2] This, combined with the 182° roll angle of the completed observation, means that the portion of the field of view with the best angular resolution (<1″, 50% encircled energy radius) lies to the west of the cluster center. In our *Chandra* images angular resolution degrades toward the east reaching ∼3″ at the edge of the S3 chip. This variation in the point spread function has negligible effect on the diffuse cluster emission; however it does influence the extent and shapes of serendipitous point sources.

The data were taken in full frame mode with a readout time of 3.2 s. Standard *Chandra* software tools were used to clean the data of time intervals with high background or bad aspect,

Figure 1: (a)—*(Left)* Composite *Chandra* X-ray image of A1995 encoding information on spectral variations in the cluster. The figure was constructed from images in three different spectral bands: 0.5–0.95 keV (*red*), 0.95–1.6 keV (*green*), and 1.6–7.5 keV (*blue*). A linear scaling was used for display, so only the bright central portion of the cluster is visible. Point sources were removed from the images before adaptive smoothing to enhance the diffuse emission. The total field of view displayed is 7.7′. (b)—*(Right)* Composite *Chandra* image of the serendipitous point sources in the vicinity of A1995 using the same spectral bands and covering the same field of view as (a). Note the great variety in the intrinsic X-ray spectra of the point sources.

remove dead or flickering pixels, and correct event gains for a focal plane temperature of −120 C. The final effective exposure time after cleaning was 54.7 ks.

3 Analysis

3.1 Diffuse Cluster Emission

Within a radius of 4′ the integrated spectrum of A1995 is well described by an absorbed thermal plasma model with temperature $kT = 7.6 \pm 0.5$ keV, metallicity 0.22 ± 0.05 times solar, and a column density $N_{\rm H} = (3.5 \pm 0.6) \times 10^{20}$ cm^{-2}. These values are consistent with the integrated spectral results from our earlier *ASCA* data. Spectra containing roughly equal numbers of counts were extracted from within three annular bins covering 0′–0.5′, 0.5′–1′, and 1′–2′. The fitted temperatures and metallicities of the individual spectra (the column density was held fixed to the globally determined value) were all consistent with the global values. Thus there is no strong radial gradient in either the temperature or metallicity and, in particular, any evidence for central cooling is weak.

In order to investigate the possibility of temperature variations on smaller spatial scales we carried out an analysis of three broad band images that contained roughly equal numbers of detected X-ray photons from the cluster. The images, binned by 4 to a scale of 1.968″ pixel^{-1}, covered the energy ranges 0.5–0.95 keV, 0.95–1.6 keV, and 1.6–7.5 keV. Exposure maps were generated at the midpoint energy of each band. Point sources were detected (see below) and removed from the images by replacing pixel values within small circular regions centered on each source with random deviates drawn from a Poisson distribution. The mean of the Poisson distribution was determined separately for each source in each spectral band by evaluating the count rate per pixel within a local annulus surrounding the source region. Thus sources superposed on bright cluster emission were replaced by higher mean rates than sources superposed on faint background emission. These images were then adaptively smoothed to an approximate signal-to-noise ratio of 10. Figure 1a shows a composite, three-color image of the diffuse cluster emission. A1995 appears predominantly as whitish, although there are a half-dozen faintly-colored regions that indicate the presence of spectral variations on spatial scales of $\sim 10''$ ($65\,h_{50}^{-1}$ kpc) near the core of the cluster. Work is ongoing to quantify the statistical significance of these apparent spectral variations and to interpret them in terms of temperature variations.

A more detailed look at the individual band data is given in Figure 2 which shows contours of X-ray surface brightness superposed on grayscale maps. The contour values in each panel have been scaled in the same manner (levels range from 0.6% to 90% of the peak emission) so that relative comparisons can be made. The shapes of the highest intensity contours show band-to-band variations that can be correlated to the color variations evident in Figure 1a. In addition an elliptical isophotal analysis yields large variations in the fitted ellipticities of the X-ray surface brightness as a function of position and spectral band within $90''$ of the cluster center. The ellipticity, defined as $a_{\rm maj}/a_{\rm min} - 1$, averages to a value of $\sim$0.3 in the inner regions of the cluster, but it varies with radius and spectral band over a broad range: 0.15 to 0.7. At larger radii ($90''$ to $200''$) the isophotal fits are very nearly the same from band to band. In all three bands there is a indication that the ellipticity increases (by +0.05) with increasing radius. The average ellipticity in these outer portions of the cluster is 0.16 at a position angle of 70°.

Image fits of 2-D elliptical isothermal-β models to the spectral band data are generally consistent with each other. This is true for the cluster center, which we determine to be $14^{\rm h}\,52^{\rm m}\,58^{\rm s}$, $58^\circ\,02'\,56''$ (J2000), as well as the fitted ellipticity, which is 0.26 at a position angle of 60°. Since the model assumes constant ellipticity, these values represent averages weighted by X-ray surface brightness and, therefore, are intermediate to the averages over the inner and outer parts of the cluster quoted above. The core radii and β (with 1 sigma statistical uncertainties) for the various bands are 0.73 ± 0.03, $44'' \pm 2''$ (0.5–0.95 keV); 0.86 ± 0.04, $53'' \pm 3''$ (0.95–1.6 keV); and 0.78 ± 0.04, $49'' \pm 3''$ (1.6–7.5 keV). The best-fitted values of β for the first and second spectral bands differ the most, by $\sim 2.6\sigma$, a result that needs to be confirmed using a more accurate model for the spatial variation of background across the S3 chip. These new *Chandra* data yield a steeper profile and larger core radius for A1995 than our earlier *ROSAT* HRI analysis did. Because of its lower effective area and higher background, the *ROSAT* HRI was really only sensitive to the bright central portions of the cluster. Thus the discrepancy in derived parameters between *Chandra* and *ROSAT* may be due to the morphological complexity of the cluster coupled with the different sensitivities of these instruments to faint diffuse emission. The range of best-fitted core radii from the *Chandra* data, $290\,h_{50}^{-1} - 350\,h_{50}^{-1}$ kpc, is consistent with other rich, non-cooling-flow clusters.

Figure 3 compares our image fits to the *Chandra* data using two quite different techniques. The panels on the left present the usual azimuthally-averaged radial surface brightness profiles of the data and model. The fitted background level (assumed uniform) and modeled cluster emission profile are shown as dashed and dotted curves, respectively. The fits are good with χ^2 values of $\sim$1 per degree of freedom. However, when radial profiles are examined on a quadrant-by-quadrant (or finer) basis, then more significant deviations between the data and model become apparent. This conclusion is further reinforced through the comparisons show in the right panels in Fig. 3, which demonstrate that there is indeed small scale spatial structure in the cluster. Here we have taken the 2-D Fast Fourier Transform of the data image with sources removed and squared and summed the resulting real and complex images to produce a power spectral density (PSD) image. This we then azimuthally-averaged in radial bins about the zero spatial frequency pixel to produce a 1-D radial PSD function. Statistical errors were propagated through this procedure. For our choice of PSD normalization, Poisson noise yields a value of 2, which is the high frequency limit shown in Fig. 3. The identical operation was applied to the model image with the addition of the noise value of 2 to the resulting 1-D radial PSD.

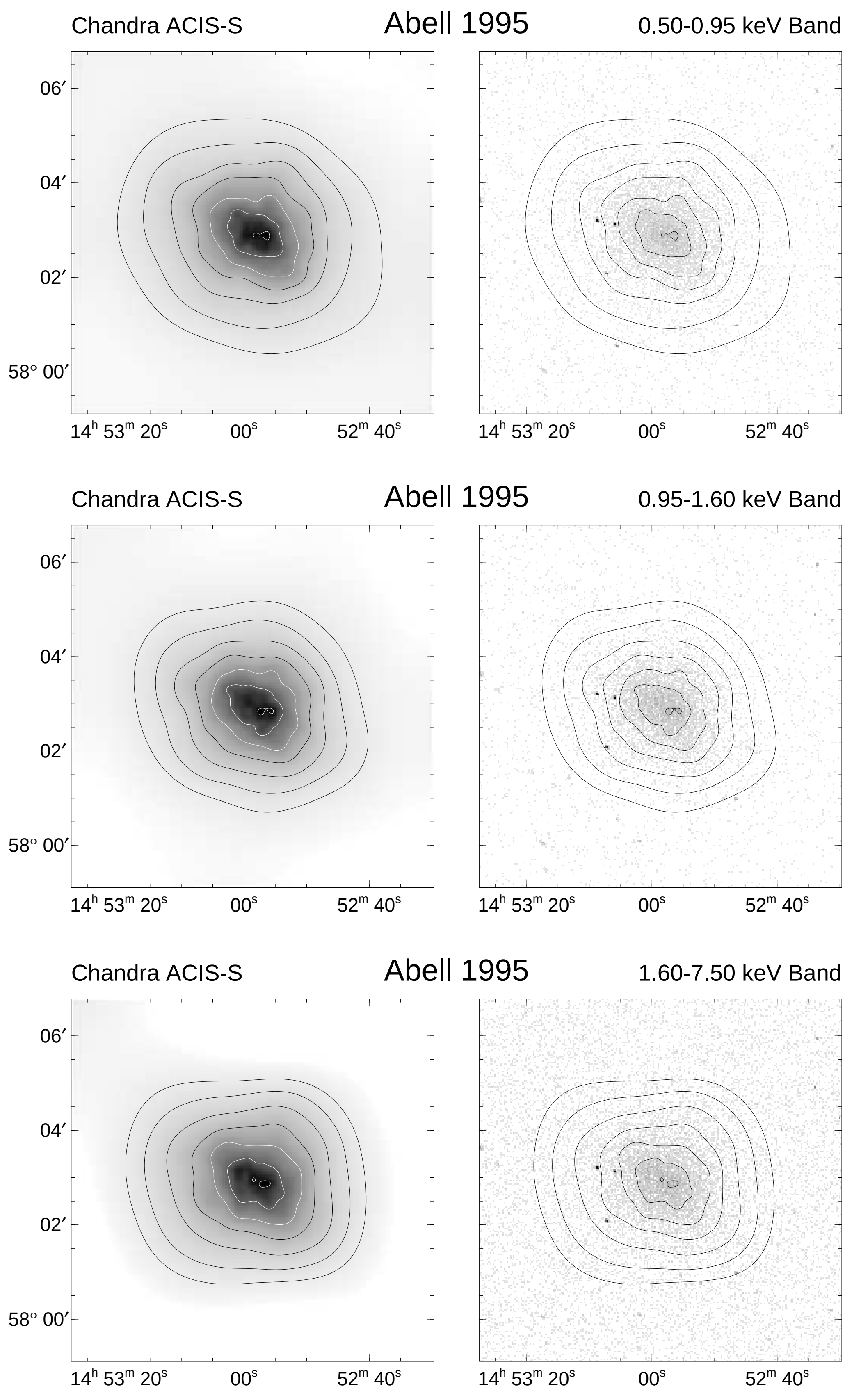

Figure 2: Contour plots superposed on grayscale images of the adaptively-smoothed diffuse cluster X-ray emission with point sources removed (*left*) and the raw *Chandra* data (*right*). Three separate energy bands 0.5–0.95 keV (*top*), 0.95–1.6 keV (*middle*), and 1.6–7.5 keV (*bottom*) are presented.

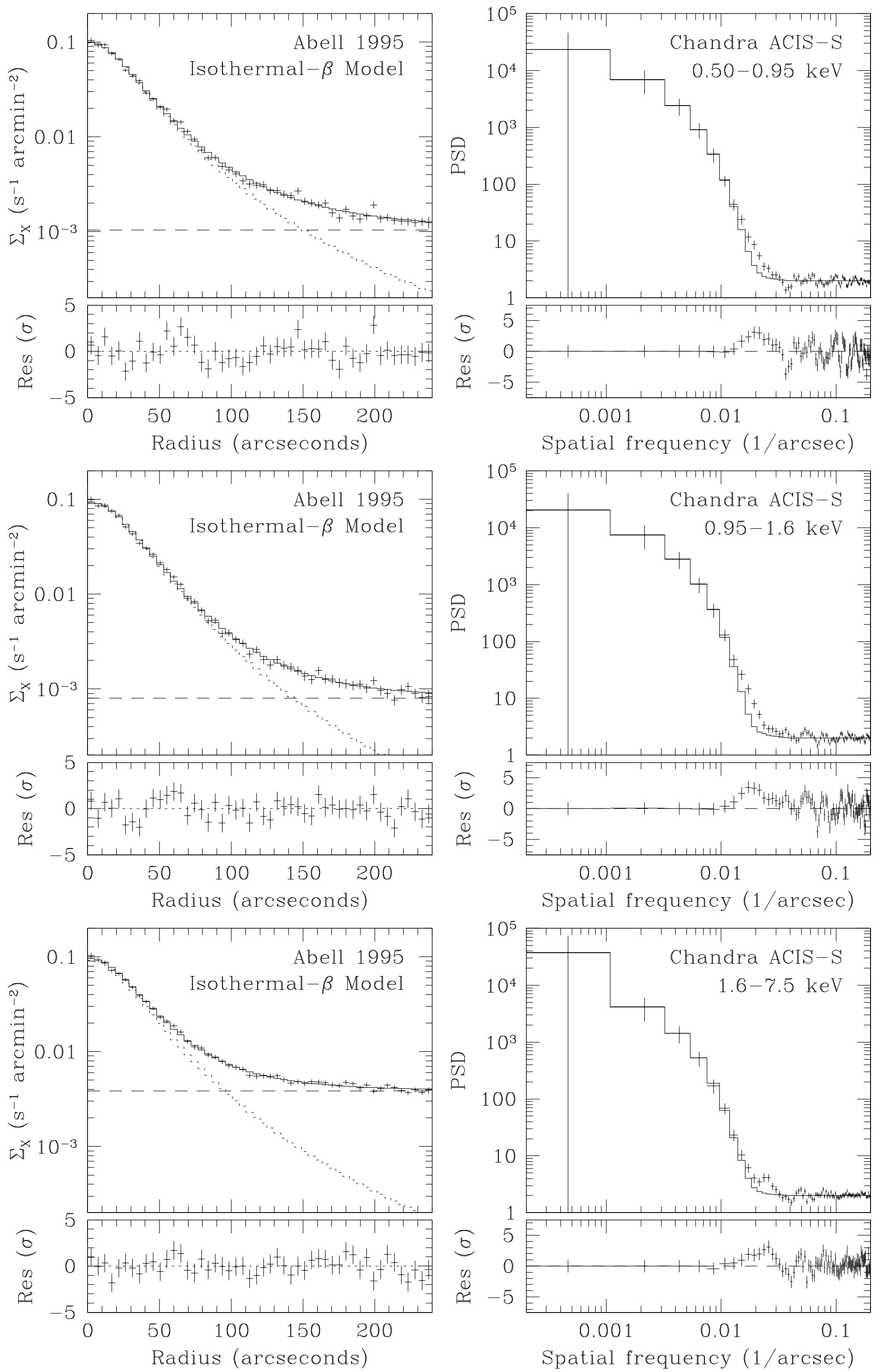

Figure 3: Comparison of 2-D elliptical isothermal-β model fits to the *Chandra* A1995 data. The left panels compare the azimuthally-averaged radial surface brightness profiles and show that the fits, at least in this sense, are good. The right panels show a comparison of the Fourier power spectral density of the model and data images, showing that the model lacks sufficient power on spatial frequencies of 0.01–0.03 arcsecond^{-1}. As before the *top*, *middle*, and *bottom* panels correspond to the three separate energy bands 0.5–0.95 keV, 0.95–1.6 keV, and 1.6–7.5 keV, respectively.

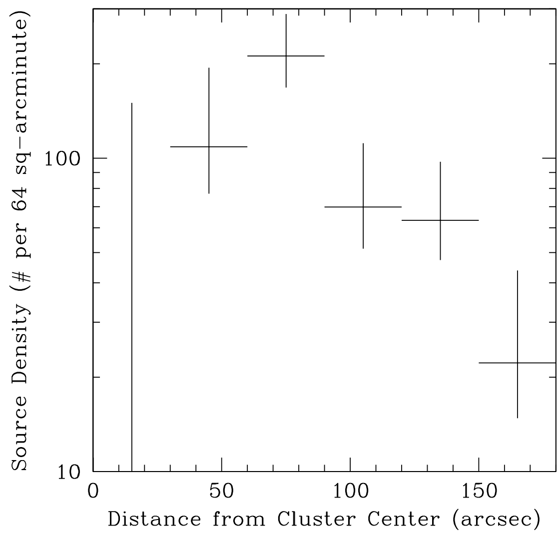

Figure 4: Radial distribution of the serendipitous X-ray point sources in the vicinity of the galaxy cluster A1995. The surface density is expressed per $8' \times 8'$ area (roughly the area of the S3 chip) and the profile is centered on the cluster. Errors are 1-sigma and were calculated assuming the source counts follow a Poisson distribution.

In all three cases the low frequency portion (below 0.01 arcsecond^{-1}) of the data and model PSDs agree well, confirming that the gross cluster shape has been well modeled. The data PSD lies significantly above the model predictions for spatial frequencies in the range 0.01–0.03 arcsecond^{-1}, indicating that there are unmodeled image structures that produce excess power on these spatial frequencies.

3.2 Serendipitous Point Sources

We detected 33 point sources in the entire field of view of the S3 chip at a statistical significance of 3-sigma or more. Twelve, 15, and 15 sources were detected at greater than 3-sigma confidence in the 0.50–0.95 keV, 0.95–1.6 keV, and 1.6–7.5 keV band images, respectively. The 0.5–7.5 keV band count rates vary from a low of 2.7×10^{-4} s^{-1} to a maximum of 0.017 s^{-1}. As demonstrated in Figure 1b, these sources show a wide range of intrinsic X-ray spectra from those with mostly soft (<1 keV) emission to others showing only hard (>1 keV) emission.

Cross-correlating the X-ray sources with the NED, SIMBAD, and USNO-A2.0 catalogs resulted in 5 matches. Two are bright stars ($m_R = 10$ and $m_R = 13$, with both showing only soft X-ray spectra), one is an IRAS galaxy ($m_R = 16.0$), and two others are unidentified stellar objects ($m_R = 18.8$ and $m_R = 19.2$). The latter two are the brightest serendipitous X-ray sources in the field and emit significantly over the entire *Chandra* band. The positions of the optical and X-ray sources agree to $<1''$, which confirms the accuracy of the *post facto* aspect solution. Using an R-band image of the A1995 field obtained by us at the Whipple Observatory 1.2-m telescope in January 1996 we determined optical counterparts for 11 X-ray sources in addition to the 5 cataloged ones. The remaining 17 X-ray sources do not show visible optical counterparts and therefore must be fainter than $m_R \sim 23$, which is the approximate magnitude limit of the image.

Recent work by Cappi et al.[3] presents evidence for an overdensity of X-ray sources in the vicinity of two rich galaxy clusters at $z \sim 0.5$. Figure 4 shows the radial surface density profile of sources in the S3 field of view for our A1995 observation binned about the center of the cluster. The dramatic decrease of the source density with distance from the cluster center indicates that we may be seeing a similar effect. Work is underway to compare the A1995 X-ray source counts to the *Chandra* deep-field counts in order to investigate this issue further.

Acknowledgments

This work was partially supported by NASA LTSA grant NAG5-3432 and *Chandra* grant GO0-1049C to JPH.

References

1. S.K. Patel *et al*, *ApJ* **541**, 37 (2000).
2. M.W. Bautz *et al*, in *Proc. SPIE Vol 3444, X-ray Optics, Instruments, and Missions*, ed. R. B. Hoover & A. B. Walker, 210.
3. M. Cappi *et al*, *ApJ* **548**, 624 (2001).